

# End-to-End Bent Perylene Bisimide Cyclophanes by Double Sulfur Extrusion

Yuki Tanaka, Keita Tajima, Ryota Kusumoto, Yasuhiro Kobori,\* Norihito Fukui,\* and Hiroshi Shinokubo\*



Cite This: *J. Am. Chem. Soc.* 2024, 146, 16332–16339



Read Online

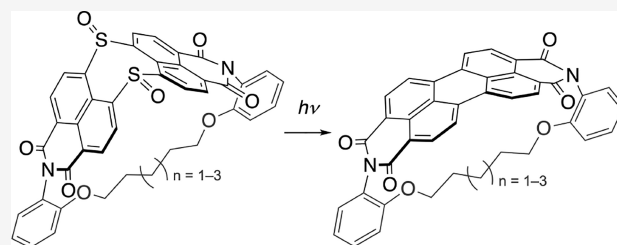
ACCESS |

Metrics & More

Article Recommendations

Supporting Information

**ABSTRACT:** Bending inherently planar  $\pi$ -cores consisting of only six-membered rings has traditionally been challenging because a powerful transformation is required to compensate for the significant strain energy associated with bending. Herein, we demonstrate that sulfur extrusion can achieve substantial molecular bending of a perylene structure to form a substructure of a Vögtle belt, a proposed yet hitherto elusive carbon nanotube fragment. Bent perylene bisimide (PBI) derivatives were synthesized through a double-sulfur-extrusion reaction from the corresponding sulfur-containing V-shaped precursors with an internal alkyl tether. The effect of bending the inherently planar PBI core, which is a recent topic of interest for the design of advanced organic electronic and optoelectronic materials, was investigated systematically. Increasing the curvature leads to a red shift in the absorption and emission spectra, while the fluorescence quantum yields remain high. This stands in contrast with the nonemissive features of previously reported nonplanar PBI derivatives based on conjugative tethers. Detailed photophysical measurements indicated that the increasing curvature with shorter alkyl tethers (i) slightly facilitates intersystem crossing and (ii) significantly suppresses the internal conversion in the excited state of the present bent PBI derivatives. The latter characteristics originate from the restricted dynamic motion associated with the charge-transfer (CT) character between the core chromophores and the *N*-aryl units.



## INTRODUCTION

Recent progress in organic synthesis has led to the development of various nonplanar  $\pi$ -conjugated molecules, which had remained elusive targets until several decades ago due to the intrinsically planar nature of  $sp^2$ -hybridized carbons.<sup>1–13</sup> To date, there have been numerous reports on bowl-shaped and warped  $\pi$ -systems in which the incorporation of non-six-membered rings induces positive or negative Gaussian curvatures.<sup>14–21</sup> However, examples of the coercive bending of inherently planar  $\pi$ -cores that consist of only six-membered rings, which have zero Gaussian curvature, remain limited because the synthesis of these contorted  $\pi$ -systems requires a powerful transformation to compensate for the significant strain energy associated with their curvature.

Representative strategies for bending  $\pi$ -systems are summarized in Figure 1.  $[n]$ Paracyclophane, the simplest model of a curved  $\pi$ -system, has been synthesized from the Dewar benzene precursor via aromatization (eq 1).<sup>22–24</sup> Bodwell and co-workers have reported the synthesis of  $\pi$ -extended cyclophanes such as pyrenophane and teropyrenophane via the electrocyclization of the corresponding cyclophanediene precursors and subsequent aromatization (eq 2).<sup>25–29</sup> Cyclo $[n]$ paraphenylenes have been prepared using two approaches: preconstruction of the main framework using  $sp^3$ -hybridized carbon atoms (eq 1)<sup>30,31</sup> and reductive

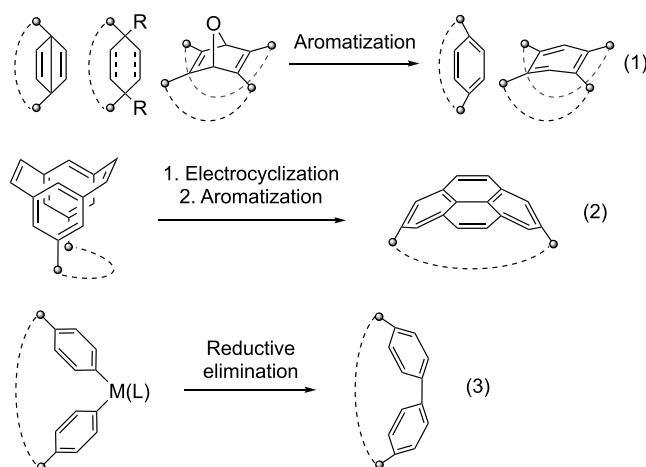


Figure 1. Strategies for the syntheses of bent  $\pi$ -systems.

Received: April 18, 2024

Revised: May 21, 2024

Accepted: May 23, 2024

Published: May 30, 2024



elimination from less-strained organometallic intermediates (eq 3).<sup>32,33</sup> The reductive-elimination strategy has also been employed to synthesize carbon nanobelts.<sup>34</sup> Recently, zigzag carbon nanobelts have been synthesized via the reductive aromatization of an oxanorbornadiene segment as the key step (eq 1).<sup>35,36</sup>

Our group has recently demonstrated that dinaphtho[1,8-*bc*:1',8'-*ef*]thiopyne bisimide (DNTBI) **1** and its sulfoxide (**2**) undergo sulfur extrusion upon electron injection, heating, or photoirradiation to yield PBI **3** almost quantitatively (Figure 2a).<sup>37,38</sup> This transformation is accompanied by the release of

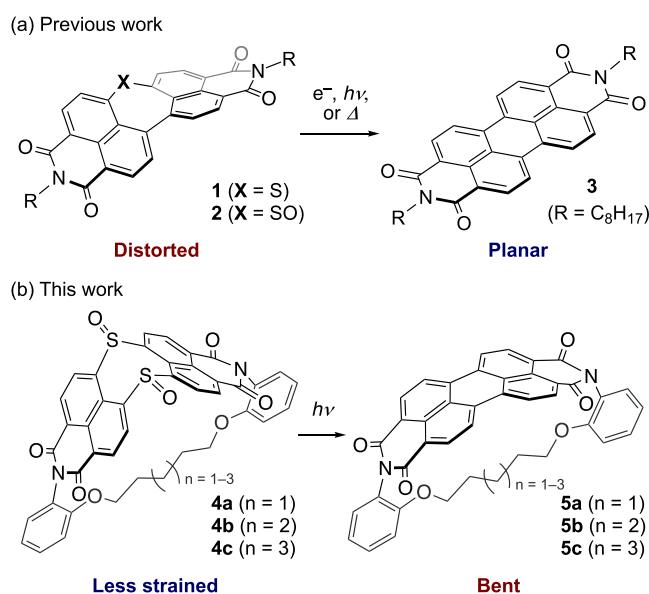


**Figure 2.** Synthesis of PBIs via sulfur-extrusion reactions from the corresponding precursors with inserted sulfur/sulfoxide units.

strain from the distorted precursors. Here, we demonstrate that PBI derivatives with two inserted sulfoxide units undergo a double-sulfur-extrusion reaction (Figure 2b). This reaction was applied to bend an inherently planar PBI core; i.e., the photoirradiation of alkyl-tethered precursors **4a–4c** afforded the corresponding (perylene bisimide)phanes (PBIphanes) **5a–5c**. The curved perylene unit represents a fragment of a Vögtle belt, which is a proposed yet hitherto elusive carbon nanotube fragment.<sup>39</sup> The molecular design of **5a–5c** was inspired by Bodwell's pyrenophanes.<sup>7,27–29</sup> While ring-contraction via sulfur extrusion from a C(sp<sup>3</sup>)–S–C(sp<sup>3</sup>) unit is a representative strategy to create cyclophanes,<sup>22</sup> the synthesis of strained molecules by sulfur extrusion from a C(sp<sup>2</sup>)–S–C(sp<sup>2</sup>) unit remains so far unprecedented.<sup>40</sup>

Figure 3 presents the previously reported PBIphanes **6–8**. Xiao and co-workers have reported **6**, which adopts contorted structures induced by  $\pi$ -conjugative linkers.<sup>41</sup> Oligoparaphenylene-tethered PBIphane **7**<sup>42</sup> and oligothiophene-tethered PBIphanes **8**<sup>43</sup> adopt twisted and planar PBI cores, respectively. Our PBIphanes **5a–5c** contain nonconjugative alkyl tethers to induce the curvature of the  $\pi$ -system. Hence, **5a–5c** should be more suitable candidates to explore the effects of the bending of inherently planar PBIs<sup>44–47</sup> on the chemical and physical properties of the  $\pi$ -conjugated cores, which has been a recent topic of high interest for the design of advanced organic electronic and optoelectronic materials.<sup>48–50</sup>

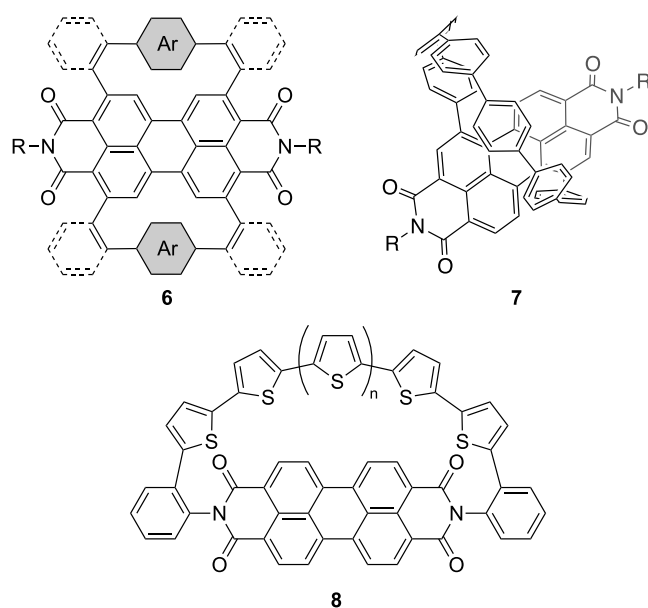


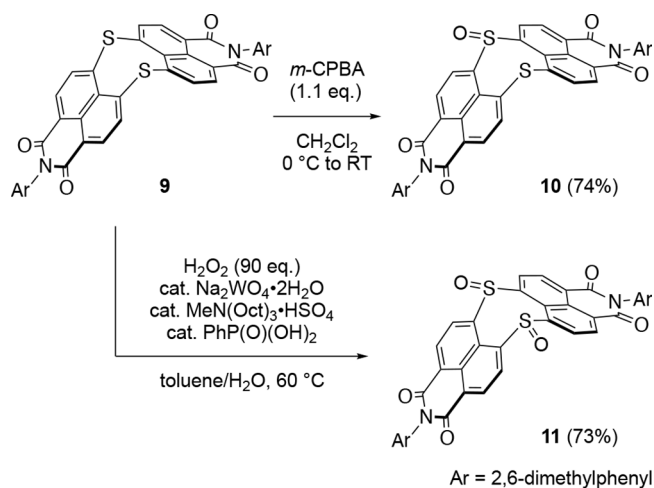
**Figure 3.** Structures of previously reported PBIphanes **6**, **7**, and **8**.

Twisted PBI derivatives with alkyl tethers have been studied by Würthner and co-workers.<sup>51,52</sup>

## RESULTS AND DISCUSSION

**Synthesis and Sulfur-Extrusion Reactions of Model Compounds.** Dinaphtho[1,8-*bc*:1',8'-*fg*][1,5]dithiocine bisimide (DNDTBI) **9**<sup>53</sup> was subjected to oxidation with *m*-chloroperbenzoic acid (*m*-CPBA, 1.1 equiv) to afford the corresponding sulfoxide **10** in 74% yield (Scheme 1). The tungsten-catalyzed oxidation<sup>54</sup> of **9** with hydrogen peroxide provided disulfoxide **11** in 73% yield.

### Scheme 1. Synthesis of Sulfoxide Derivatives of DNDTBI



The solid-state structures of **10** and **11** were unambiguously determined by using single-crystal X-ray diffraction analysis (Figure 4). In the crystal, **10** and **11** adopt a V-shaped structure similar to that of **9**. The interplanar angles between the two naphthalene monoimide units gradually decrease in the order **9** (113°) > **10** (100°) > **11** (94°) due to the smaller bond angle of sulfoxide compared to that of sulfide. The distances between the *ortho*-substituents of the *N*-aryl groups

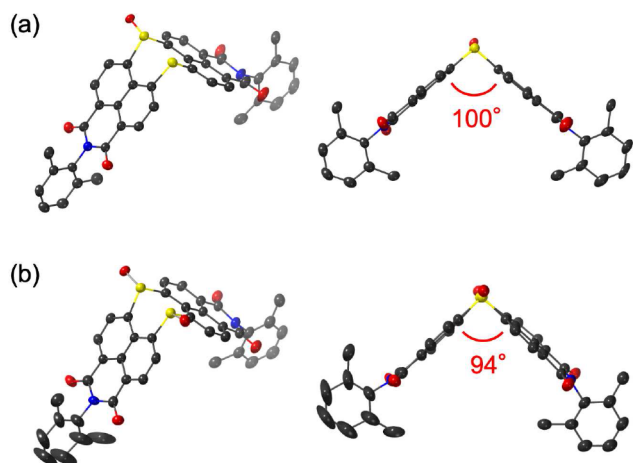


**Figure 4.** X-ray crystal structures of (a) **10** and (b) **11** with thermal ellipsoids at 50% probability; all hydrogen atoms have been omitted for the sake of clarity.

of **9**, **10**, and **11** are 11.0, 9.2–9.8, and 8.2 Å, respectively. These values are comparable to the O–O distance of 1,6-hexanediol (8.7 Å) and longer than that of 1,5-pentanediol (7.3 Å).

The UV/vis absorption spectra of **9**–**11** are shown in Figure 5. DNDTBI **9** exhibits a broad absorption band at 450 nm,

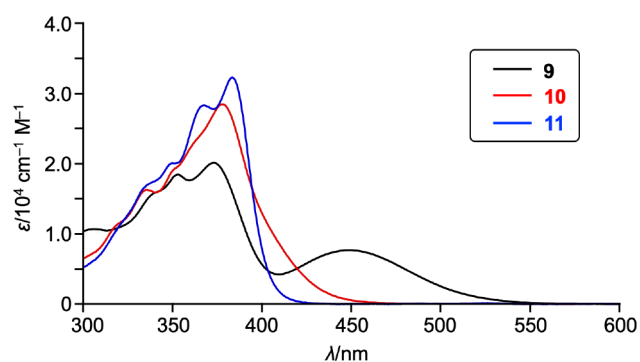


**Figure 5.** UV/vis absorption spectra of **9**–**11** in  $\text{CH}_2\text{Cl}_2$ ;  $\lambda$ , wavelength;  $\epsilon$ , extinction coefficient.

which was assigned to the charge-transfer (CT) transition from the central sulfur atoms to the naphthalene monoimide units.<sup>53</sup> Accordingly, monosulfoxide **10** shows hypsochromically shifted absorption with a shoulder peak tailing to 460 nm. Furthermore, the CT transition completely disappeared in the absorption spectrum of **11**, with the remaining sharp absorption bands tailing at 420 nm.

Subsequently, we examined the photoinduced sulfur-extrusion reactions of **9**–**11** in  $\text{CH}_2\text{Cl}_2$  (Figure 6). Photoirradiation was performed using a high-pressure mercury lamp equipped with a sharp cutoff filter ( $\lambda > 380$  nm). Compound **9** underwent the sulfur-extrusion reaction, albeit sluggishly, to afford PBI **3'** in only 19% yield even after an extended photoirradiation period of 3 h. In contrast, the sulfur-extrusion reaction of **10** afforded PBI **3'** almost quantitatively within 900 s. Notably, a broad absorption band appeared at 370–450 nm during the irradiation of **10**. This feature resembles the spectrum of DNTBI **1** rather than that of its sulfoxide **2**. These results suggest that the sulfoxide unit rather than the sulfide unit of **10** was removed preferentially, which is in agreement

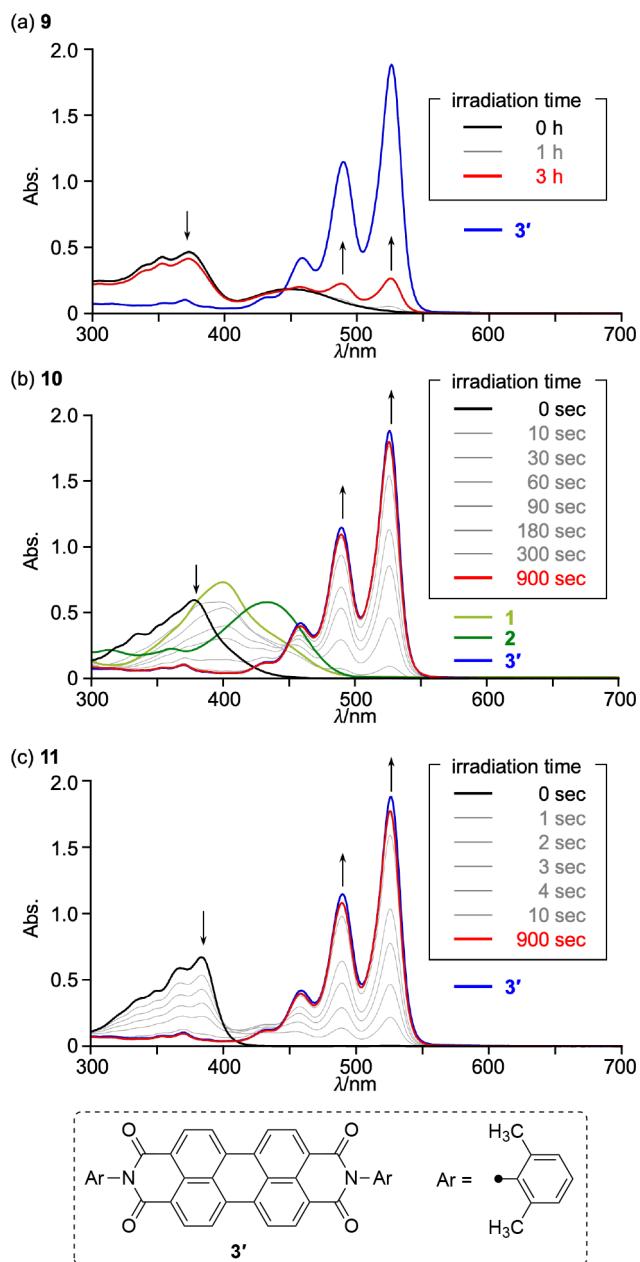


**Figure 6.** Changes in the UV/vis absorption spectra of (a) **9**, (b) **10**, and (c) **11** upon photoirradiation in  $\text{CH}_2\text{Cl}_2$ . A high-pressure mercury lamp equipped with a sharp cutoff filter ( $\lambda > 380$  nm) was employed for the photoirradiation;  $[1] = [2] = [3'] = [9]_0 = [10]_0 = [11]_0 = 2.1 \times 10^{-5} \text{ M}^{-1}$ .

with the observed trend for **1** and **2**, i.e., the sulfur-extrusion reaction of **2** proceeded more rapidly than that of **1**.<sup>38</sup> Furthermore, the sulfur-extrusion reaction of **11** was faster than that of **10**, reaching completion to give **3'** in approximately 30 s. After 15 min of photoirradiation, the absorption spectrum is almost identical to that of PBI **3'**, indicating nearly quantitative conversion. The lack of isosbestic points can be attributed to the formation of DNTBI sulfoxide **2** as an intermediate.

We also examined the sulfur-extrusion reaction of **11** via electron injection or heating. The cyclic voltammograms of **11** in  $\text{CH}_2\text{Cl}_2$  (Figure S39) feature an irreversible reduction wave at  $-1.38$  V in the forward direction. Upon backsweeping, two peaks were observed at  $-0.97$  and  $-1.16$  V, which are identical

## Scheme 2. Synthesis of PBIphanes 5a–5c

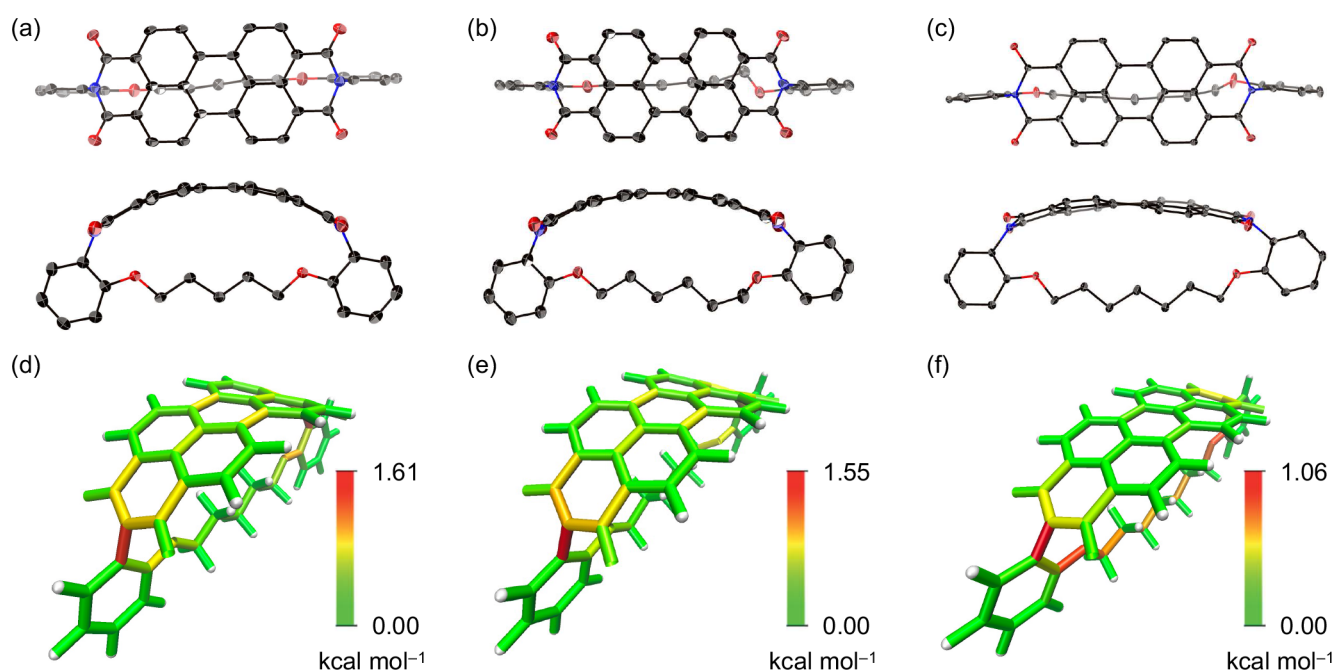
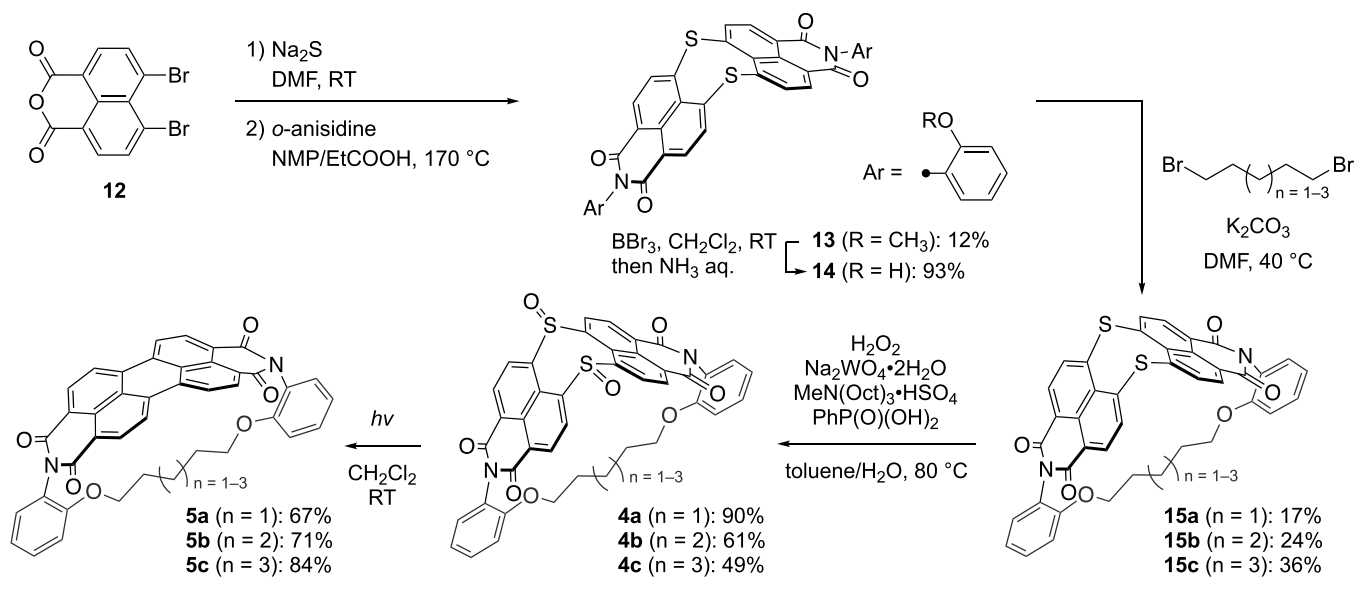


**Figure 7.** X-ray crystal structures (top: top view; bottom: side view) of (a) **5a**, (b) **5b**, and (c) **5c** with thermal ellipsoids at 50% probability; all hydrogen atoms are omitted for clarity. Visualized local strains in (d) **5a**, (e) **5b**, and (f) **5c** were calculated at the B3LYP/6-31G(d) level.

to those of PBI **3'**. Furthermore, spectroelectrochemical measurements of **11** revealed that the absorption spectrum of **11** after electrochemical reduction is identical to that of the radical anion of PBI **3'** (Figure S40). These results indicate that electron injection triggers the extrusion of sulfur from **11**, as was observed for the previously reported DNTBI sulfoxide **2**. On the other hand, the thermogravimetric analysis (TGA) profile of **11** exhibits no characteristic mass decrease due to sulfur extrusion while DNTBI sulfoxide **2** underwent sulfur extrusion upon heating (Figure S42).

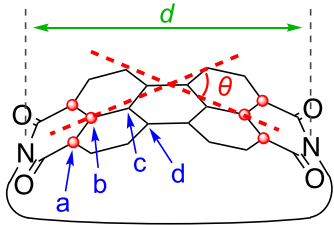
**Synthesis of PBIphanes.** The synthesis of PBIphanes **5a–5c** is shown in Scheme 2. In our previous procedure, a 4,5-dibromonaphthalic monoimide derivative was subjected to a nucleophilic aromatic substitution ( $\text{S}_{\text{N}}\text{Ar}$ ) reaction with  $\text{Na}_2\text{S}$  to afford DNTBI **9**.<sup>53</sup> Here, we attempted to treat 4,5-

dibromo-1,8-naphthalic anhydride **12** with *o*-anisidine; however, this resulted in an undesired competing  $\text{S}_{\text{N}}\text{Ar}$  reaction at the bromo substituents. We thus conducted the initial  $\text{S}_{\text{N}}\text{Ar}$  reaction of **12** with  $\text{Na}_2\text{S}$  and subsequent treatment with *o*-anisidine afforded *o*-anisyl DNTBI **13** in 12% yield. The aryl oxygen groups of **13** were deprotected with  $\text{BBr}_3$  to furnish 2-hydroxyphenyl DNTBI **14** in 93% yield. Treatment of **14** with 1,5-dibromopentane, 1,6-dibromohexane, or 1,7-dibromoheptane provided the corresponding internally tethered products **15a**, **15b**, and **15c** in 17, 24, and 36% yield, respectively. The sulfide units of **15a**, **15b**, and **15c** were converted to sulfoxides through tungsten-catalyzed oxidation to give **4a**, **4b**, and **4c** in 90, 61, and 49% yield, respectively. Finally, photoirradiation of **4a**, **4b**, and **4c** with a high-pressure mercury lamp afforded the

desired PBIphanes **5a**, **5b**, and **5c** in 67, 71, and 84% yield, respectively.

The structures of PBIphanes **5a–5c** were unambiguously determined by X-ray diffraction analysis (Figure 7a–c). Structural parameters are summarized in Table 1. In the single

**Table 1. Structural Parameters and Calculated Strain Energies for **5a–5c****



	$d^a/\text{\AA}$	$\theta^b/^\circ$	POAV angle/ $^\circ$				$E^c/\text{kcal mol}^{-1}$
			a	b	c	d	
<b>5a</b>	10.55	33.8	3.2	1.2	1.2	2.2	22.9
<b>5b</b>	10.78	29.4	2.6	1.2	1.5	2.0	19.7
<b>5c</b>	11.15	19.4	2.0	0.6	0.7	1.0	17.4

<sup>a</sup>Nitrogen–nitrogen distance. <sup>b</sup>End-to-end bend angle. <sup>c</sup>Strain energy.

crystal, PBIphanes **5a**, **5b**, and **5c** adopt bent structures with nitrogen–nitrogen distances,  $d$ , of 10.55, 10.78, and 11.15 Å, respectively. These nitrogen–nitrogen distances are significantly shorter than that of planar PBI **3** ( $d = 11.3$  Å)<sup>55</sup> and comparable to those of previously reported contorted PBIphanes **6** ( $d = 10.25$ – $11.36$  Å). The end-to-end bend angles,  $\theta$ , are 33.8° (**5a**), 29.4° (**5b**), and 19.4° (**5c**). In the X-ray crystal structure of **5b**, one methylene unit neighboring an oxygen atom adopts a gauche configuration, which can be attributed to the mismatch due to having an even-numbered alkyl chain as the tethering unit. The  $\pi$ -orbital-axis-vector (POAV) angles,<sup>56</sup> which provide a measure of the degree of orbital hybridization based on structural aspects, were calculated based on the crystal structures of **5a–5c** (Table 1), in which the obtained POAV angles at the equivalent carbons were averaged. The POAV angles increase in the order **5c** < **5b** < **5a**, indicating that increased curvature decreases the s-character of the constituent carbon atoms. The deviation from planarity is most pronounced at the imide-substituted carbon atoms (position a).

The strain energies in **5a**, **5b**, and **5c** were investigated using hypothetical homodesmotic reactions at the B3LYP/6-31G(d) level and were calculated to be 22.9, 19.7, and 13.6 kcal mol<sup>-1</sup>, respectively (Figure S45). The local strain energies were also visualized using the StrainVis tool (Figure 7d–f).<sup>57</sup> The PBIphanes **5a**, **5b**, and **5c** exhibit the greatest local strain at the C–N bond of the *N*-aryl substituents, which increases with decreasing length of the alkyl linker (**5a**: 1.61 kcal mol<sup>-1</sup>; **5b**: 1.55 kcal mol<sup>-1</sup>; **5c**: 1.06 kcal mol<sup>-1</sup>). In the perylene core, the strain is mainly localized at the peripheral bonds around the naphthalene segments, as was also observed in a computational simulation of a Vögtle belt.<sup>57</sup> The C–O bonds in **5a–5c** also contribute substantially to the accommodation of the local strain.

The solubility value of **5a** in CHCl<sub>3</sub> (0.11 mg/mL) is higher than those of **5b** (0.027 mg/mL) and **5c** (0.045 mg/mL), due to the large molecular curvature. However, these solubility values of PBIphanes **5a–5c** are smaller than that of planar *N*-

(2-methoxyphenyl)-substituted PBI **3''** (0.38 mg/mL), which exhibits high solubility due to the existence of rotamers. The relatively low solubility of PBIphanes **5a–5c** is attributable to the restricted rotation of their *N*-substituents.

**Aromaticity of PBIphanes.** In the <sup>1</sup>H NMR spectra of **5a–5c** and untethered planar PBI **3''** in tetrachloroethane-*d*<sub>2</sub>, the signals of the aromatic protons showed an upfield shift with increasing curvature (**5a**: 8.64 and 8.62 ppm; **5b**: 8.67 and 8.65 ppm; **5c**: 8.71 and 8.69 ppm; **3''**: 8.74 and 8.72 ppm). DFT calculations reproduced this trend (Table S3). Nevertheless, the nucleus-independent chemical shift (NICS) values at the carbonyl-substituted six-membered rings of **5a–5c** and **3''**, which represent an averaged value among four rings, are almost comparable (**5a**: –6.44 ppm; **5b**: –6.44 ppm; **5c**: –6.52 ppm; **3''**: –6.61 ppm). Consequently, we conclude that (i) increasing the molecular curvature in PBI has a negligible effect on the aromaticity and (ii) the observed upfield shifts of the aromatic proton signals originate from the change in orientation toward the neighboring carbonyl group or aromatic ring.

**Electrochemical Properties of PBIphanes.** The cyclic voltammograms and differential pulse voltammograms of **5a–5c** and **3''** were measured in CH<sub>2</sub>Cl<sub>2</sub> by using 0.1 M Bu<sub>4</sub>NPF<sub>6</sub> as the supporting electrolyte and Ag/AgNO<sub>3</sub> as the reference electrode (Figure S41). The ferrocene/ferrocenium couple (Fc/Fc<sup>+</sup>) was used as an internal reference. For **5a–5c** and **3''**, two reversible reduction waves (**5a**: –1.03 and –1.27 V; **5b**: –1.01 and –1.24 V; **5c**: –1.00 and –1.23 V; and **3''**: –1.03 and –1.22 V) were observed. These results indicate that the sensitivity of the CV measurements is insufficient to distinguish the subtle effect of molecular bending on the electron-accepting abilities.

**Photophysical Properties of PBIphanes.** The UV/vis absorption and emission spectra of PBI **3''** and PBIphanes **5a–5c** are shown in Figure 8, and their photophysical parameters are summarized in Table 2. Increasing the structural curvature of the PBI cores results in a red shift of the longest-wavelength absorption peaks from 527 nm (**3''**) to 544 nm (**5a**), together with decreased extinction coefficients. This trend contrasts with those of pyrenophane and teropyrenophane, in which increased structural curvature leads to blue-shifted absorption spectra.<sup>26,28</sup> These results firmly corroborate the recent argument that the symmetry of the local orbitals in the K-region (bonding or antibonding) governs the (de)stabilization of the HOMO and LUMO.<sup>50</sup> The shortest-wavelength emission peaks also exhibited a bathochromic shift from 535 nm (**3''**) to 555 nm (**5a**) with increasing curvature. The PBIphanes exhibited intense emission with quantum yields,  $\Phi_F$ , of 0.84–0.88, which are larger than that of planar PBI **3''** ( $\Phi_F = 0.76$ ). It is worth noting here that the previously reported  $\pi$ -tethered contorted PBI derivatives **6** exhibit behavior that is different from that of the present PBIphanes **5a–5c**: (i) negligible correlation between the absorption wavelength and molecular bending and (ii) weak emission ( $\Phi_F = 0.01$ – $0.32$ )<sup>41</sup>; these differences highlight the fact that the electronic properties of **6** are substantially altered by the  $\pi$ -delocalization onto the tethering  $\pi$ -linkers.

The full widths at half-maximum (fwhm's) of the 0–0 absorption bands of **5a**, **5b**, **5c**, and **3''** calculated from the Gauss fitting are 659, 686, 661, and 601 cm<sup>-1</sup>, respectively. The Stokes shifts of **5a**, **5b**, **5c**, and **3''** are 364, 403, 344, and 284 cm<sup>-1</sup>, respectively. The larger fwhm and Stokes shift values of PBIphanes **5a–5c** compared to those of planar PBI **3''** were

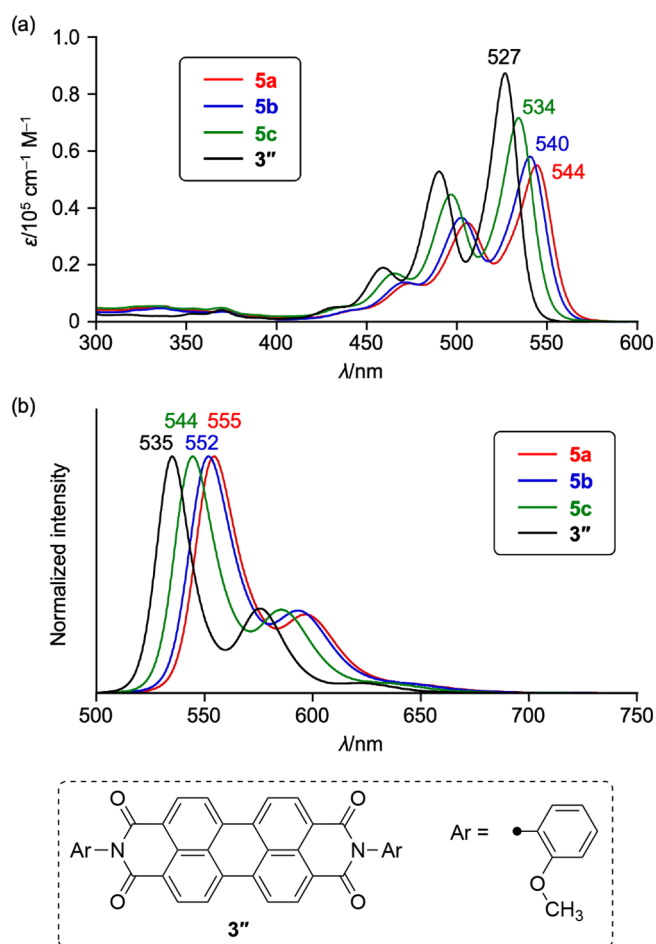


**Figure 8.** UV-vis (a) absorption and (b) emission spectra of **3''**, **5a**, **5b**, and **5c** in  $\text{CHCl}_3$ ;  $\lambda$ , wavelength; and  $\epsilon$ , extinction coefficient.

**Table 2. Photophysical Parameters of **3''** and **5a–5c****

	$\Delta\nu^a/\text{cm}^{-1}$	$\Phi_F^b$	$\Phi_{\text{ISC}}^c$	$\tau_F^d/\text{ns}$	$k_r^e/10^8 \text{ s}^{-1}$	$k_{\text{nr}}^f/10^8 \text{ s}^{-1}$
<b>5a</b>	364	0.88		4.9	1.8	0.24
<b>5b</b>	403	0.84	0.001	4.6	1.8	0.35
<b>5c</b>	344	0.84	0.002	4.1	2.0	0.39
<b>3''</b>	284	0.76		3.6	2.1	0.67

<sup>a</sup>Stokes shift. <sup>b</sup>Fluorescence quantum yield. <sup>c</sup>ISC quantum yield. <sup>d</sup>Fluorescence lifetime. <sup>e</sup>Radiative decay constant. <sup>f</sup>Nonradiative decay constant.

attributed to their nonplanar structures. Interestingly, the fwhm and Stokes shift values of **5b** are larger than those of **5a** and **5c**, suggesting that the mismatch of its even-numbered alkyl chain increases the structural flexibility.

The photophysical parameters of **5a–5c** and **3** are summarized in Table 2. Their radiative decay rates,  $k_r$ , decrease slightly from  $2.1 \times 10^8$  to  $1.8 \times 10^8 \text{ s}^{-1}$  with increasing structural curvature. TD-DFT calculations at the CAM-B3LYP/6-31G(d) level indicated that the oscillator strength of the  $S_0$ – $S_1$  transitions also decreases in the same order (**3**: 0.96 > **5c**: 0.78 > **5b**: 0.70 > **5a**: 0.67) (Figure S46), which is in agreement with their extinction coefficients. These results can be explained by the decreased HOMO–LUMO overlap with increasing curvature. The increase in structural curvature also decreases the nonradiative decay rates,  $k_{\text{nr}}$ , from  $0.67 \times 10^8$  to  $0.24 \times 10^8 \text{ s}^{-1}$ . Transition-absorption spectroscopy measurements indicated that the photoexcitation

of **5b** and **5c** affords long-lived species with lifetimes of 86 and 125  $\mu\text{s}$ , which were assigned to the triplet excited states (Figure S47). The intersystem crossing (ISC) quantum yield values,  $\Phi_{\text{ISC}}$ , of **5b** and **5c** are 0.1 and 0.2%, respectively (Figure S48). These  $\Phi_{\text{ISC}}$  values are greater than the reported triplet yield of *N,N'*-bis(2,5-di-*tert*-butylphenyl)-substituted PBI **3'''** ( $\Phi_{\text{ISC}} < 10^{-4}$ ),<sup>58</sup> indicating that the molecular bending promotes ISC.<sup>59</sup> However, the  $\Phi_{\text{ISC}}$  values are in general very low, indicating that the nonradiative deactivation of the bent PBIs **5a–5c** mainly proceeds through internal conversion (IC). Using the reported fluorescence yield and decay of PBI **3'''**, its IC rate constant was estimated to be  $k_{\text{nr}} = 3 \times 10^6 \text{ s}^{-1}$ , which is approximately one-tenth of those of **5a–5c**. TD-DFT calculations of **5a–5c** also indicated the charge-transfer (CT) character between the core chromophores and the aryl units as the second excited state ( $S_2$ ) in the  $S_0$ -optimized geometries (Figure S46). Thus, the disordered motion in the alkyl linker is anticipated to cause a vibronic admixture between  $S_1$  and  $S_2$  to promote the IC processes to the  $S_0$  states via CT character. Indeed, the  $\Phi_F$  values in toluene (**3''**: 87%; **5a**: 90%; **5b**: 86%; **5c**: 87%) are larger than those in  $\text{CHCl}_3$ . Furthermore, the fact that the  $k_{\text{nr}}$  value of **5c** is greater than those of **5a** and **5b** strongly supports this hypothesis, because the flexibility of the alkyl chain linker increases with increasing length, allowing the orbital hybridization between HOMO and HOMO–1 as shown in Figure S46. In contrast, shorter linkages restrict the aforementioned orbital overlap due to the more rigid geometry. However, the  $k_{\text{nr}}$  value in **5a** is greater than that in **3'''**, indicating that the alkyl linkages essentially induce vibronic coupling for the nonradiative processes.

## CONCLUSIONS

We have described the synthesis and properties of bent PBI derivatives **5a–5c**, which feature an internal alkyl chain tethering the two *N*-aryl substituents. These PBIphanes were synthesized via sulfur-extrusion reactions from corresponding disulfide precursors **4a–4c**. X-ray diffraction analysis of **5a–5c** demonstrated that their degree of curvature increases with decreasing length of the alkyl tether. The strain energy was evaluated to be as high as 22.9 kcal mol<sup>−1</sup> (**5a**) based on homodesmotic reactions. The <sup>1</sup>H NMR analysis of **5a–5c** indicated that the aromatic proton signals were shifted upfield by approximately 0.1 ppm with increasing molecular curvature. This shift is due to the change in orientation toward the neighboring carbonyl group or aromatic ring rather than a change in aromaticity. Electrochemical measurements of **5a–5c** indicated that increasing the molecular curvature in PBI has a negligible effect on electron affinity. In sharp contrast, the increased curvature leads to a red shift of the absorption and emission spectra (by ~20 nm), while the high fluorescence quantum yields (up to 88%) are maintained. This behavior contrasts with the nonemissive features of previously reported contorted  $\pi$ -extended PBI derivatives **6**. Detailed photophysical measurements of **5a–5c** indicated that the nonradiative deactivation of the  $S_1$  state via IC is suppressed by the restricted dynamic motion associated with the CT character between the core chromophores and the *N*-aryl units. Our results demonstrate that the double-sulfur-extrusion reactions enable the construction of curved perylene structures and the effect that the structural curvature exerts on the structural, electrochemical, and photophysical properties of these PBIs. These findings can be expected to find applications in the design of advanced organic materials.

## ■ ASSOCIATED CONTENT

## SI Supporting Information

The Supporting Information is available free of charge at <https://pubs.acs.org/doi/10.1021/jacs.4c05358>.

Experimental details and spectral data for all new compounds (PDF)

## Accession Codes

CCDC 2348376–2348380 contain the supplementary crystallographic data for this paper. These data can be obtained free of charge via [www.ccdc.cam.ac.uk/data\\_request/cif](http://www.ccdc.cam.ac.uk/data_request/cif), or by emailing [data\\_request@ccdc.cam.ac.uk](mailto:data_request@ccdc.cam.ac.uk), or by contacting The Cambridge Crystallographic Data Centre, 12 Union Road, Cambridge CB2 1EZ, UK; fax: +44 1223 336033.

## ■ AUTHOR INFORMATION

## Corresponding Authors

Yasuhiro Kobori – Department of Chemistry, Graduate School of Science and Molecular Photoscience Research Center, Kobe University, Kobe 657-8501, Japan; CREST, JST, Kawaguchi, Saitama 332-0012, Japan; [orcid.org/0000-0001-8370-9362](https://orcid.org/0000-0001-8370-9362); Email: [ykobori@kitty.kobe-u.ac.jp](mailto:ykobori@kitty.kobe-u.ac.jp)

Norihito Fukui – Department of Molecular and Macromolecular Chemistry, Graduate School of Engineering, and Integrated Research Consortium on Chemical Science (IRCCS), Nagoya University, Nagoya, Aichi 464-8603, Japan; PRESTO, Japan Science and Technology Agency (JST), Kawaguchi, Saitama 332-0012, Japan; [orcid.org/0000-0002-0466-0116](https://orcid.org/0000-0002-0466-0116); Email: [fukui@chembio.nagoya-u.ac.jp](mailto:fukui@chembio.nagoya-u.ac.jp)

Hiroshi Shinokubo – Department of Molecular and Macromolecular Chemistry, Graduate School of Engineering, and Integrated Research Consortium on Chemical Science (IRCCS), Nagoya University, Nagoya, Aichi 464-8603, Japan; [orcid.org/0000-0002-5321-2205](https://orcid.org/0000-0002-5321-2205); Email: [hshino@chembio.nagoya-u.ac.jp](mailto:hshino@chembio.nagoya-u.ac.jp)

## Authors

Yuki Tanaka – Department of Molecular and Macromolecular Chemistry, Graduate School of Engineering, and Integrated Research Consortium on Chemical Science (IRCCS), Nagoya University, Nagoya, Aichi 464-8603, Japan

Keita Tajima – Department of Molecular and Macromolecular Chemistry, Graduate School of Engineering, and Integrated Research Consortium on Chemical Science (IRCCS), Nagoya University, Nagoya, Aichi 464-8603, Japan

Ryota Kusumoto – Department of Chemistry, Graduate School of Science, Kobe University, Kobe 657-8501, Japan

Complete contact information is available at: <https://pubs.acs.org/doi/10.1021/jacs.4c05358>

## Notes

The authors declare no competing financial interest.

## ■ ACKNOWLEDGMENTS

This work was supported by JSPS KAKENHI grants JP20H05862 (H.S. and N.F.), JP20H05863 (H.S.), JP20H05867 (N.F.), JP22K14663 (N.F.), and JP23H03947 (N.F.), as well as JST, PRESTO grant JPMJPR21Q7 (N.F.). This paper is dedicated to Prof. Atsuhiko Osuka on the occasion of his 70th birthday.

## ■ REFERENCES

- (1) Gingras, M. One Hundred Years of Helicene Chemistry. Part 3: Applications and Properties of Carbohelicenes. *Chem. Soc. Rev.* **2013**, *42*, 1051–1095.
- (2) Scott, L. T. Methods for the Chemical Synthesis of Fullerenes. *Angew. Chem., Int. Ed.* **2004**, *43*, 4994–5007.
- (3) Kawase, T.; Kurata, H. Ball-, Bowl-, and Belt-Shaped Conjugated Systems and Their Complexing Abilities: Exploration of the Concave–Convex  $\pi$ – $\pi$  Interaction. *Chem. Rev.* **2006**, *106*, 5250–5273.
- (4) Wu, Y.-T.; Siegel, J. S. Aromatic Molecular-Bowl Hydrocarbons: Synthetic Derivatives, Their Structures, and Physical Properties. *Chem. Rev.* **2006**, *106*, 4843–4867.
- (5) Pascal, R. A. Twisted Acenes. *Chem. Rev.* **2006**, *106*, 4809–4819.
- (6) Shen, Y.; Chen, C.-F. Helicenes: Synthesis and Applications. *Chem. Rev.* **2012**, *112*, 1463–1535.
- (7) Bodwell, G. J. Extraordinary Transformations to Achieve the Synthesis of Remarkable Aromatic Compounds. *Chem. Rec.* **2014**, *14*, 547–567.
- (8) Miao, Q. Heptagons in Aromatics: From Monocyclic to Polycyclic. *Chem. Rec.* **2015**, *15*, 1156–1159.
- (9) Segawa, Y.; Yagi, A.; Matsui, K.; Itami, K. Design and Synthesis of Carbon Nanotube Segments. *Angew. Chem., Int. Ed.* **2016**, *55*, 5136–5158.
- (10) Hiroto, S. Innovative Synthesis and Functions of Curved  $\pi$ -Conjugated Molecules. *Bull. Chem. Soc. Jpn.* **2018**, *91*, 829–838.
- (11) Saito, M.; Shinokubo, H.; Sakurai, H. Figuration of Bowl-shaped  $\pi$ -Conjugated Molecules: Properties and Functions. *Mater. Chem. Front.* **2018**, *2*, 635–661.
- (12) Márquez, I. R.; Castro-Fernández, S.; Millán, A.; Campaña, A. G. Synthesis of Distorted Nanographenes Containing Seven- and Eight-membered Carbocycles. *Chem. Commun.* **2018**, *54*, 6705–6718.
- (13) Majewski, M. A.; Stępień, M. Bowls, Hoops, and Saddles: Synthetic Approaches to Curved Aromatic Molecules. *Angew. Chem., Int. Ed.* **2019**, *58*, 86–116.
- (14) Barth, W. E.; Lawton, R. G. Dibenzo[ghi,mno]fluoranthene. *J. Am. Chem. Soc.* **1966**, *88*, 380–381.
- (15) Scott, L. T.; Jackson, E. A.; Zhang, Q.; Steinberg, B. D.; Bancu, M.; Li, B. A Short, Rigid, Structurally Pure Carbon Nanotube by Stepwise Chemical Synthesis. *J. Am. Chem. Soc.* **2012**, *134*, 107–110.
- (16) Feng, C.-N.; Kuo, M.-Y.; Wu, Y.-T. Synthesis, Structural Analysis, and Properties of [8]Circulenes. *Angew. Chem., Int. Ed.* **2013**, *52*, 7791–7794.
- (17) Sakamoto, Y.; Suzuki, T. Tetrabenzo[8]circulene: Aromatic Saddles from Negatively Curved Graphene. *J. Am. Chem. Soc.* **2013**, *135*, 14074–14077.
- (18) Yamamoto, K.; Harada, T.; Okamoto, Y.; Chikamatsu, H.; Nakazaki, M.; Kai, Y.; Nakao, T.; Tanaka, M.; Harada, S.; Kasai, N. Synthesis and Molecular Structure of [7]Circulene. *J. Am. Chem. Soc.* **1988**, *110*, 3578–3584.
- (19) Luo, J.; Xu, X.; Mao, R.; Miao, Q. Curved Polycyclic Aromatic Molecules That Are  $\pi$ -Isoelectronic to Hexabenzocoronene. *J. Am. Chem. Soc.* **2012**, *134*, 13796–13803.
- (20) Kawasumi, K.; Zhang, Q.; Segawa, Y.; Scott, L. T.; Itami, K. A Grossly Warped Nanographene and the Consequences of Multiple Odd-membered-ring Defects. *Nat. Chem.* **2013**, *5*, 739–744.
- (21) Fukui, N.; Kim, T.; Kim, D.; Osuka, A. Porphyrin Arch-Tapes: Synthesis, Contorted Structures, and Full Conjugation. *J. Am. Chem. Soc.* **2017**, *139*, 9075–9088.
- (22) Kane, V. V.; De Wolf, W. H.; Bickelhaupt, F. Synthesis of Small Cyclophanes. *Tetrahedron* **1994**, *50*, 4575–4622.
- (23) Jenneskens, L. W.; de Kanter, F. J. J.; Kraakman, P. A.; Turkenburg, L. A. M.; Koolhaas, W. E.; de Wolf, W. H.; Bickelhaupt, F.; Tobe, Y.; Kakiuchi, K.; Odaira, Y. [5]Paracyclophane. *J. Am. Chem. Soc.* **1985**, *107*, 3716–3717.
- (24) Tobe, Y.; Kawaguchi, M.; Kakiuchi, K.; Naemura, K. [2.2]Orthoparacyclophane: The Last and Most Strained [2.2]Cyclophane. *J. Am. Chem. Soc.* **1993**, *115*, 1173–1174.

- (25) Bodwell, G. J.; Bridson, J. N.; Houghton, T. J.; Kennedy, J. W. J.; Mannion, M. R. 1,8-Dioxo[8](2,7)pyrenophane, a Severely Distorted Polycyclic Aromatic Hydrocarbon. *Angew. Chem., Int. Ed.* **1996**, *35*, 1320–1321.
- (26) Bodwell, G. J.; Bridson, J. N.; Cyrański, M. K.; Kennedy, J. W. J.; Krygowski, T. M.; Mannion, M. R.; Miller, D. O. Nonplanar Aromatic Compounds. 8<sup>1</sup> Synthesis, Crystal Structures, and Aromaticity Investigations of the 1,*n*-Dioxo[*n*](2,7)pyrenophanes. How Does Bending Affect the Cyclic  $\pi$ -Electron Delocalization of the Pyrene System? *J. Org. Chem.* **2003**, *68*, 2089–2098.
- (27) Merner, B. L.; Dawe, L. N.; Bodwell, G. J. 1,1,8,8-Tetramethyl[8](2,11)teropyrenophane: Half of an Aromatic Belt and a Segment of an (8,8) Single-Walled Carbon Nanotube. *Angew. Chem., Int. Ed.* **2009**, *48*, 5487–5491.
- (28) Merner, B. L.; Unikela, K. S.; Dawe, L. N.; Thompson, D. W.; Bodwell, G. J. 1,1,*n,n*-Tetramethyl[*n*](2,11)teropyrenophanes (*n* = 7–9): A Series of Armchair SWCNT Segments. *Chem. Commun.* **2013**, *49*, 5930–5932.
- (29) Unikela, K. S.; Roemmele, T. L.; Houska, V.; McGrath, K. E.; Tobin, D. M.; Dawe, L. N.; Boeré, R. T.; Bodwell, G. J. Gram-Scale Synthesis and Highly Regioselective Bromination of 1,1,9,9-Tetramethyl[9](2,11)teropyrenophane. *Angew. Chem., Int. Ed.* **2018**, *57*, 1707–1711.
- (30) Jasti, R.; Bhattacharjee, J.; Neaton, J. B.; Bertozzi, C. R. Synthesis, Characterization, and Theory of [9]-, [12]-, and [18]-Cycloparaphenylene: Carbon Nanohoop Structures. *J. Am. Chem. Soc.* **2008**, *130*, 17646–17647.
- (31) Takaba, H.; Omachi, H.; Yamamoto, Y.; Bouffard, J.; Itami, K. Selective Synthesis of [12]Cycloparaphenylene. *Angew. Chem., Int. Ed.* **2009**, *48*, 6112–6116.
- (32) Yamago, S.; Watanabe, Y.; Iwamoto, T. Synthesis of [8]Cycloparaphenylene from a Square-Shaped Tetranuclear Platinum Complex. *Angew. Chem., Int. Ed.* **2010**, *49*, 757–759.
- (33) Tsuchido, Y.; Abe, R.; Ide, T.; Osakada, K. A Macrocyclic Gold(I)–Biphenylene Complex: Triangular Molecular Structure with Twisted Au<sub>2</sub>(diphosphine) Corners and Reductive Elimination of [6]Cycloparaphenylene. *Angew. Chem., Int. Ed.* **2020**, *59*, 22928–22932.
- (34) Povie, G.; Segawa, Y.; Nishihara, T.; Miyauchi, Y.; Itami, K. Synthesis of a Carbon Nanobelt. *Science* **2017**, *356*, 172–175.
- (35) Cheung, K. Y.; Watanabe, K.; Segawa, Y.; Itami, K. Synthesis of a Zigzag Carbon Nanobelt. *Nat. Chem.* **2021**, *13*, 255–259.
- (36) Han, Y.; Dong, S.; Shao, J.; Fan, W.; Chi, C. Synthesis of a Sidewall Fragment of a (12,0) Carbon Nanobelt. *Angew. Chem., Int. Ed.* **2021**, *60*, 2658–2662.
- (37) Hayakawa, S.; Matsuo, K.; Yamada, H.; Fukui, N.; Shinokubo, H. Dinaphthothiepine Bisimide and Its Sulfoxide: Soluble Precursors for Perylene Bisimide. *J. Am. Chem. Soc.* **2020**, *142*, 11663–11668.
- (38) Tanaka, Y.; Matsuo, K.; Yamada, H.; Fukui, N.; Shinokubo, H. Gram-Scale Diversity-Oriented Synthesis of Dinaphthothiepine Bisimides as Soluble Precursors for Perylene Bisimides. *Eur. J. Org. Chem.* **2022**, *2022*, No. e202200770.
- (39) Vögtle, F.; Schröder, A.; Karbach, D. Strategy for the Synthesis of Tube-Shaped Molecules. *Angew. Chem., Int. Ed. Engl.* **1991**, *30*, 575–577.
- (40) Lewis, S. E. Cycloparaphenylenes and Related Nanohoops. *Chem. Soc. Rev.* **2015**, *44*, 2221–2304.
- (41) Liu, T.; Yang, J.; Geyer, F.; Conrad-Burton, F. S.; Hernández Sánchez, R.; Li, H.; Zhu, X.; Nuckolls, C. P.; Steigerwald, M. L.; Xiao, S. Stringing the Perylene Diimide Bow. *Angew. Chem., Int. Ed.* **2020**, *59*, 14303–14307.
- (42) Li, A.; Zhang, X.; Wang, S.; Wei, K.; Du, P. Synthesis and Physical Properties of a Perylene Diimide-Embedded Chiral Conjugated Macrocyclic. *Org. Lett.* **2023**, *25*, 1183–1187.
- (43) Bold, K.; Stolte, M.; Shoyama, K.; Krause, A.; Schmiedel, A.; Holzapfel, M.; Lambert, C.; Würthner, F. Macrocyclic Donor-Acceptor Dyads Composed of Oligothiophene Half-Cycles and Perylene Bisimides. *Chem. – Eur. J.* **2022**, *28*, No. e202200355.
- (44) Würthner, F. Perylene Bisimide Dyes as Versatile Building Blocks for Functional Supramolecular Architectures. *Chem. Commun.* **2004**, 1564–1579.
- (45) Weil, T.; Vosch, T.; Hofkens, J.; Peneva, K.; Müllen, K. The Rylene Colorant Family—Tailored Nanoemitters for Photonics Research and Applications. *Angew. Chem., Int. Ed.* **2010**, *49*, 9068–9093.
- (46) Zhan, X.; Facchetti, A.; Barlow, S.; Marks, T. J.; Ratner, M. A.; Wasielewski, M. R.; Marder, S. R. Rylene and Related Diimides for Organic Electronics. *Adv. Mater.* **2011**, *23*, 268–284.
- (47) Würthner, F.; Saha-Möllner, C.; Fimmel, B.; Ogi, S.; Leowanawat, P.; Schmidt, D. Perylene Bisimide Dye Assemblies as Archetype Functional Supramolecular Materials. *Chem. Rev.* **2016**, *116*, 962–1052.
- (48) Conrad-Burton, F. S.; Liu, T.; Geyer, F.; Costantini, R.; Schlaus, A. P.; Spencer, M. S.; Wang, J.; Hernández Sánchez, R.; Zhang, B.; Xu, Q.; Steigerwald, M. L.; Xiao, S.; Li, H.; Nuckolls, C. P.; Zhu, X. Controlling Singlet Fission by Molecular Contortion. *J. Am. Chem. Soc.* **2019**, *141*, 13143–13147.
- (49) Schaaack, C.; Evans, A. M.; Ng, F.; Steigerwald, M. L.; Nuckolls, C. High-Performance Organic Electronic Materials by Contorting Perylene Diimides. *J. Am. Chem. Soc.* **2022**, *144*, 42–51.
- (50) Cruz, C. M.; Walsh, J. C.; Juríček, M. Bending Pyrenacenes to Fill Gaps in Singlet-Fission-Based Solar Cells. *Org. Mater.* **2022**, *4*, 163–169.
- (51) Osswald, P.; Würthner, F. Conformational Effects of Bay Substituents on Optical, Electrochemical and Dynamic Properties of Perylene Bisimides: Macrocyclic Derivatives as Effective Probes. *Chem.—Eur. J.* **2007**, *13*, 7395–7409.
- (52) Weh, M.; Rühle, J.; Herbert, B.; Krause, A.-M.; Würthner, F. Deracemization of Carbohelices by a Chiral Perylene Bisimide Cyclophane Template Catalyst. *Angew. Chem., Int. Ed.* **2021**, *60*, 15323–15327.
- (53) Tanaka, Y.; Tajima, K.; Fukui, N.; Shinokubo, H. Dinaphtho-[1,8-*bc*:1',8'-*fg*][1,5]dithiocine Bisimide. *Asian J. Org. Chem.* **2021**, *10*, 541–544.
- (54) Sato, K.; Hyodo, M.; Aoki, M.; Zheng, X.-Q.; Noyori, R. Oxidation of Sulfides to Sulfoxides and Sulfones with 30% Hydrogen Peroxide under Organic Solvent- and Halogen-Free Conditions. *Tetrahedron* **2001**, *57*, 2469–2476.
- (55) Briseno, A. L.; Mannsfeld, S. C. B.; Reese, C.; Hancock, J. M.; Xiong, Y.; Jenekhe, S. A.; Bao, Z.; Xia, Y. Perylenediimide Nanowires and Their Use in Fabricating Field-Effect Transistors and Complementary Inverters. *Nano Lett.* **2007**, *7*, 2847–2853.
- (56) Haddon, R. C. Rehybridization and  $\pi$ -Orbital Overlap in Nonplanar Conjugated Organic Molecules:  $\pi$ -Orbital Axis Vector (POAV) Analysis and Three-dimensional Hückel Molecular Orbital (3D-HMO) Theory. *J. Am. Chem. Soc.* **1987**, *109*, 1676–1685.
- (57) Colwell, C. E.; Price, T. W.; Stauch, T.; Jasti, R. Strain Visualization for Strained Molecules. *Chem. Sci.* **2020**, *11*, 3923–3930.
- (58) Ford, W. E.; Kamat, P. V. Photochemistry of 3,4,9,10-perylenetetracarboxylic dianhydride dyes. 3. Singlet and triplet excited-state properties of the bis(2,5-di-*tert*-butylphenyl)imide derivative. *J. Phys. Chem.* **1987**, *91*, 6373–6380.
- (59) Nagarajan, K.; Mallia, A. R.; Muraleedharan, K.; Hariharan, M. Enhanced Intersystem Crossing in Core-twisted Aromatics. *Chem. Sci.* **2017**, *8*, 1776–1782.